Hindawi
Geofluids
Volume 2022, Article ID 6464564, 19 pages
https://doi.org/10.1155/2022/6464564

Research Article

Application and Research of Gangue Partial-Filling Mining Method in Preventing Water Inrush from Floor

Zhenzhong Pang,[1,2] Xinguo Zhang,[3] Juntao Chen,[3] and Feifan Li[4]

[1]*Collage of Geoscience and Surveying Engineering, China University of Mining & Technology, Beijing 100083, China*
[2]*National Engineering Research Center of Coal Mine Water Hazard Controlling, Beijing 100083, China*
[3]*College of Energy and Mining Engineering, Shandong University of Science and Technology, Qingdao 266590, China*
[4]*Inner Mongolia Gucheng Mining Co., Ltd, Zhungeer Banner, 016215, China*

Correspondence should be addressed to Xinguo Zhang; pzz17864292900@163.com

Received 14 September 2021; Revised 7 November 2021; Accepted 24 February 2022; Published 21 March 2022

Academic Editor: Jianwei Cheng

Coal gangue produced during coal production not only poses a serious threat to the ground environment but also imposes serious economic burdens on the mine. The partial-filling mining (PFM) method proposed in this paper can make full use of coal gangue and is of great significance to the prevention and control of water disasters at the working face. The specific process used to implement this method is to first divide the working face into several narrow working faces and then fill the filling body into part of the goaf. The ability of PFM to restrain floor water inrush is analyzed by physical simulation, and the field application research is carried out at the No. 9211 mining face of Bucun Coal Mine in Shandong, China. The physical simulation results show that the failure depth of this layer is less than 5 m. The field measurements reveal that the maximum compression deformation of the filling body is 89.1 mm, and the maximum floor failure depth of the floor is only 8.6 m. Comparative analysis indicates that the floor failure depth of the No. 9211 working face with the local filling method is 4.6 m lower than that of the No. 9110 working face with the strip mining method. In addition, no water inrush accident occurs at the No. 9211 working face during mining. Therefore, PFM not only controls the floor damage depth effectively but also consumes coal gangue to protect the mine environment.

1. Introduction

In recent years, coal, as an important energy source, has made important contributions to China's economic development. However, due to the increasingly complex geological conditions encountered during coal resource excavation, there are many "secondary disasters" in mines, such as water inrush accidents, rock bursts, roof fall accidents, surface subsidence, and the creation of surface gangue hills [1–4]. These "secondary disasters" have had important impacts on continued mining development. In mining, mine water is not only a groundwater resource but also a potential threat that has become more important due to increases in mining depths and therefore the hydraulic pressures [5, 6]. More than 25 billion tons of coal resources are at risk of water inrush from the floor, especially in deep Permo-Carboniferous coal seams in the central and eastern parts of northern China [7–11]. Therefore, determining how to exploit resources threatened by a floor water inrush is an important main problem for scientific researchers and is important to continued mine development. The formation of water-conducting channels is the main cause of water inrush accidents under the premise of determining the water abundance and filling intensity of aquifers. Therefore, it is necessary to prevent and control the formation of water-conducting channels.

The formation of water-conducting channels is affected by many factors. The dynamic failure process and prevention measures have been investigated using the following approaches. First, several floor rock fracture evolution theories have been developed based on the theory of elastic-plastic mechanics. These include the under three-zone

theory, the strong seepage theory, and the rock-water stress relationship theory [12–15].

Second, the formation and evolution of water-conducting channels under the combined action of rock pressure and confined water have been analyzed via numerical and physical simulations. For example, Cao et al. [16] established a numerical calculation model of roof collapse column water inrush using UDEC software and studied the influence of mining on roof collapse column water inrush. Lu and Wang [17] analyzed the control effects of propulsion distance, rock heterogeneity, and water pressure on inrushing water via numerical simulations. Liu et al. [18] proposed a new formation microscanning imaging method such that the results could directly reflect subtle changes in wellbore fractures. They used UDEC software to simulate the process by which water flow from fractured-zone height evolves. Zhang and Meng [19] analyzed coal seam floor failure using a self-developed simulation model of confined aquifer strata.

Third, geographic information systems and microseismic (MS) monitoring techniques have been used to predict and evaluate the dangerous parts of a water-conducting channel. For example, Chen et al. [20] used a geographic information system and an analytic hierarchy to forecast the areas at risk of a water inrush in the Qidong Coal Mine. This guided the safe mining of a coal seam. Gu et al. [21] established an evaluation model based on water blocking conditions and used two adjacent lower coal mining faces of the Yanzhou Xinglongzhuang coal mine as an example. The evaluation showed that the impermeability strength is a better index for measuring the water resistance capacity of a floor. Sun et al. [22] studied fault-zone occurrence using the electric couple method. Naghadehi et al. [23] established a fuzzy model by combining FAHP with AHP applying the method to the Jajarm bauxite mine in Iran and ranked the most suitable mining methods.

Finally, ground drilling, grouting, drainage or decompression, and curtain closure have been used to prevent the formation of water-conducting channels. Guo et al. [24] thought that plugging grouting is the most effective water inrush treatment scheme in the case of water inrush. Liu et al. [25] used concrete-based curtain grouting closures for mine flood prevention and control. Li et al. [6] applied rock beam theory to analyze the mechanism of grouting crack expansion caused by rock deformation during mining and proposed a new grouting casing model designed to prevent water inrush and therefore control floor rock deformation.

Thus, scientific researchers have performed detailed studies of dynamic damage due to diversion channels and the measures that might prevent the formation of these channels. These meaningful results are a useful reference for understanding water inrush mechanisms and for the application of appropriate measures to prevent and control water inrush. However, stress in the rock surrounding a roadway and the confined water pressure of an aquifer increase linearly with the mining depth. The water control measures used in mining a shallow coal seam may be inadequate for deep-water control. Moreover, the cost and difficulty of constructing such measures increase with depth, and the equilibrium between the groundwater and the ecosystem is destroyed [26–30]. Therefore, further in-depth research into methods of preventing and controlling water inrush into mines is needed.

In summary, there have been many detailed studies of dynamic failure among diversion channels and methods of preventing the formation of such channels. According to the "under three-zone" theory, controlling the heights of the floor failure and pressure conduction zones is an important step in improving the effective thickness of the complete rock strata. The empirical formula for the floor failure depth developed by domestic researchers indicates that reducing the inclined length of a working face can reduce the floor failure depth. Therefore, a short-wall mining face is important to reduce the floor damage depth. At the same time, as a green mining method, filling mining reduces not only the supporting stress around the excavation face but also the number of gangue hills, helping to protect the mine environment. Therefore, partial-filling mining (PFM), which is a combination of short-wall mining and filling mining, is proposed to prevent the formation of water diversion channels.

2. Engineering Geological Conditions

2.1. Engineering Geology Overview. The Bucun Coal Mine is located in Zhangqiu District, Jinan City, Shandong Province, China (Figure 1). The research object is 9211 working face in 921 mining area of 9-1 coal seam threatened by floor confined water. Seven faults were exposed in the 9211 working face tunneling process; no fault affects the working face during excavation. Thus, the influence of the fault structure on mining is not considered in this study. The 9211 working face coal seam thickness is 1.0 m–1.8 m, the average thickness is 1.5 m, the coal seam dip angle is 3°–14°, the average dip angle is 9.5°, the coal seam burial depth is 506 m–571.7 m, and the average burial depth is 538.9 m. The direct bottom of the 9-1 coal seam is fine sandstone, and the basic bottom is sandy shale. The layout of the working face in the mining area is shown in Figure 2.

2.2. Hydrological Conditions. The aquifers that affect mining of the 9211 working face mainly include the upper Carboniferous thin limestone IV(V) aquifer group, the middle Carboniferous Benxi Xujiazhuang limestone aquifer group, and the Ordovician limestone aquifer group. The upper Carboniferous thin limestone IV(V) aquifer group was drained during mining. Mining of the No. 9-1 coal seam is affected mainly by the Xujiazhuang limestone aquifer group in the Middle Carboniferous Benxi formation and Ordovician limestone aquifer group in the lower part of the coal seam. The Xujiazhuang limestone aquifer group is rich in water; some areas receive a vertical overflow recharge from the Ordovician limestone aquifer group. The average distance from the 9-1 coal seam is 58.01 m, the unit water inflow is 7.2 m^3/h–246 m^3/h, the water level is -128.3 m–46.8 m, and the water pressure is 4.11 MPa. The Ordovician limestone aquifer group is located in the basement of the coal measure strata and is the most important aquifer in this area, which is 88.87 m away from the 9-1 coal seam. According to the Ordovician limestone long observation data, the highest

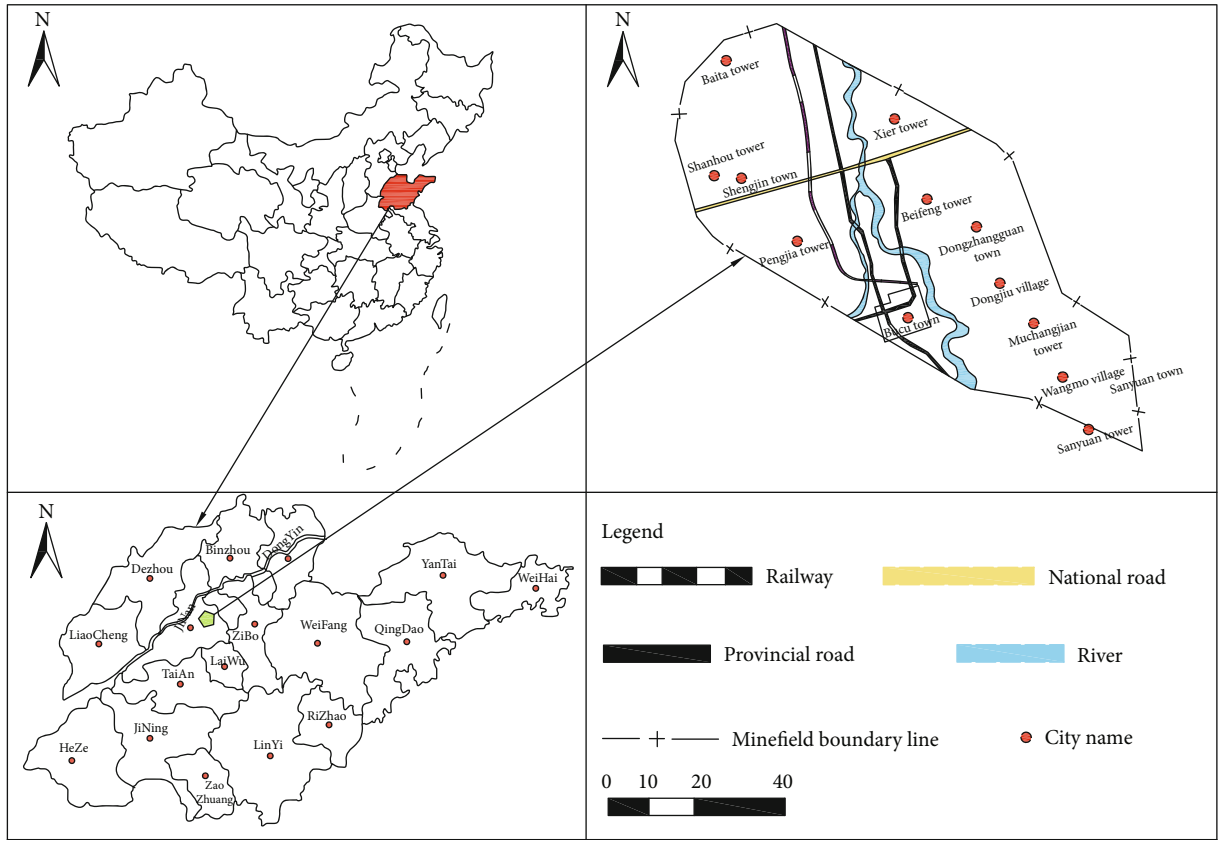

Figure 1: Location of the study area in Zhangqiu District, China.

water level is 78.34 m, the lowest water level is 47.82 m, and the Ordovician limestone water pressure is 4.87 MPa. The histogram is shown in Figure 3.

2.3. Analysis of a Water Inrush Accident. According to the analysis in Sections 2.1 and 2.2, the No. 9-1 coal seam is under threat of floor water inrush during mining. To reduce the floor damage depth at the working face, short-wall strip mining is adopted for the No. 9110 working face during coal seam mining. The mining width of the working face strip is 40 m. The working face advances along the trend of the coal seam. In order to determine the depth of floor failure when strip mining is adopted, the double-end water shutoff device observation method is used to measure the floor failure depth. On July 7, mining of the No. 9110 working face began in the Bucun Coal Mine. Deep observation of floor damage began on July 10. According to the summary of the mine pressure laws of other working faces provided by the field staff, it is believed that the initial pressure appears when the 9110 working face is pushed to July 27. However, according to the mine pressure theory, the initial pressure can cause flood accidents easily. In order to avoid potential personal injury from such an accident, observation work ended on July 27. According to the analysis of drilling leakage data, the failure depth of the working face floor reaches 13 m. It should be noted that this depth cannot represent the maximum failure depth of the floor as the working face advances. The depth continues to change as the working face advances. On July 31, the basic roof of the No. 9110 working face breaks and a water inrush accident occurs in the coal seam floor. The initial and maximum (stable) rates of water inflow are 150 m^3/h and 351.6 m^3/h, respectively. A map of the water inrush accident at the No. 9110 working face is shown in Figure 4.

Water prevention and control experts performed a detailed analysis of the factors that affected the water inrush accident at the No. 9110 working face. The results are as follows.

2.3.1. The Working Face Inclined Length. In order to prevent a water inrush accident from occurring at the working face, traditional long-wall mining was abandoned when working face 9110 was mined. The No. 9110 working face was mined using short-wall strip mining. However, water inrushes still occurred at the back of the goaf in the course of advancing. This shows that safe mining of the working face cannot be ensured when the inclined length of the working face is 40 m.

2.3.2. The Damage Depth of the Floor. The No. 9110 working face water inrush accident occurred during the initial pressure. The main reason for this is that the initial pressure increases the floor damage depth. The remaining undamaged floor thickness cannot resist the effect of the confined water pressure. Finally, the water inrush accident occurs at the working faces under the coupled effects of the initial pressure and the confined water pressure. Therefore, on

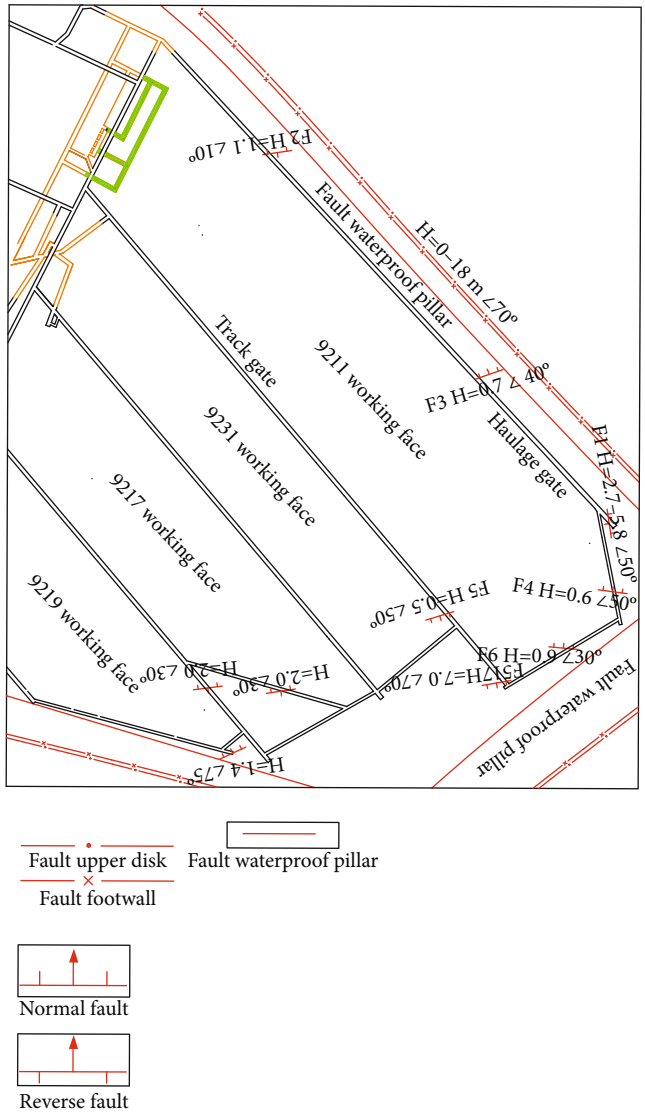

Figure 2: Working face layout in the Bucun Coal Mine.

Stratigraphic unit			Columnar legend	Lithology	Thickness (m)	Hydrogeological property
System	Series	Formation				
Carboniferous	Upper series	Taiyuan formation		Three limestone	0.90	Aquifer
				Sandy shale	14.10	Aquiclude
				Four limestone	1.00	Aquifer
				Fine-grained sandstone	4.90	Aquiclude
				Sandy shale	6.70	
				Five limestone	1.76	Aquifer
				9_{-1} mine	1.87	
				Fine-grained sandstone	8.60	Aquiclude
				Sandy shale	12.42	
				10_{-1} mine	1.25	
				Clay shale	2.25	Aquiclude
				Sandy shale	4.00	
				Fine-grained sandstone	4.13	
				Clay shale	4.97	
				Sandy shale	7.10	
				10_{-2} mine	0.60	
				Clay shale	6.30	Aquiclude
				Sandy shale	4.20	
				10_{-3} mine	0.95	
				Clay shale	3.90	Aquiclude
	Middle series	Benxi formation		Sandy shale	2.46	
				Fine-grained sandstone	5.13	
				Xujiazhuang-limestone	27.70	Aquifer
				Shale	4.00	Aquiclude
Ordovician	Middle series	Badou fundation		Ordovician limestone	820	Aquifer

Figure 3: The histogram.

the premise of determining the thickness of floor aquifuge, reducing the depth of floor failure is required in order to prevent floor water inrush.

2.3.3. The Geological Structure. The borehole data shows that the geological structure in the lower part of the No. 9110 working face is well developed. Because faults and fault zones destroy aquifuge integrity, the water resistance capacity is reduced. At the same time, it is easy to change the hydraulic conductivity of the original fault via primary and periodic pressure. Therefore, under the premise of determining the geological structure of the coal seam floor, reducing the influences of the initial pressure and periodic pressure on the fault can help to control floor water inrush.

3. Methodology

3.1. Mining Methods and Filling Materials. According to the analysis of the water inrush at the No. 9110 working face in Section 2.3, selection of a reasonable mining method and working face inclined length is important to controlling the formation of a water inrush passage. These measures can reduce the occurrence of mine water inrush accidents. However, in coal seam mining, different mining methods have different destruction depths. PFM, which is a combination of short-wall mining and filling mining, may prevent the formation of a water-conducting channel. In this method, the pressure from the overlying strata is transferred to the floor. This prevents the floor from moving to the goaf via a composite support system comprised of the roof plus backfill plus a stratum. In short-wall mining, the working face is divided into narrow-strip faces with two safety exits. The distance between the strip faces must be less than the limit span of the roof stratum to ensure that the roof undergoes only bending deformation. In filling mining, the goaf of the working face is filled to ensure that the roof of the goaf does not subside.

Using PFM, the working face was first divided into narrow-strip faces with widths of 15 m along the coal seam strike after the coal mining system of the No. 9211 working

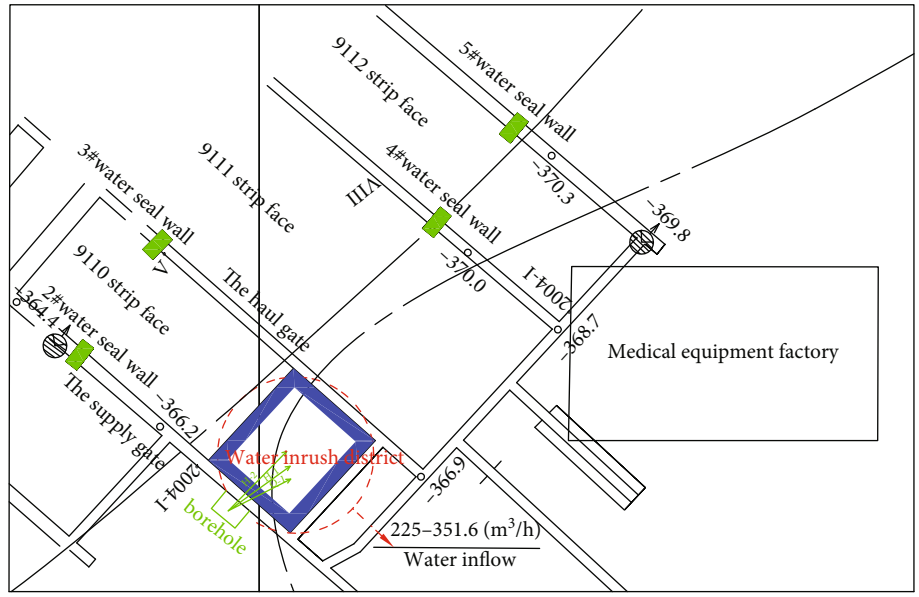

Figure 4: Map of the water inrush accident at the No. 9110 working face.

face was established. The narrow-strip faces were numbered from 1 to 15. The working face advanced along the coal seam tendency via blasting. Full negative pressure ventilation was adopted for the coalface. Figure 5 shows the PFM process, which is as follows:

(1) Face No. 1 was first extracted via blasting. Then, a preventing-grout wall was built at the upper and lower outlets of the narrow working face. When the preventing-grout wall was complete, the slurry was filled into the goaf via a pipeline from the upper exit of the strip face. This continued until all of the odd-numbered narrow-strip faces were excavated and filled

(2) When the compressive strength of the filling bodies was large enough, the coal pillars between the filling bodies were excavated in order

(3) The second cycle of PFM described above could also occur once the strength of the filling bodies in the first, third, and fifth zones was self-supporting, thus saving the process replacement time between the first and second cycles

The filling material used in the Bucun coal mine was composed mainly of aggregate, binders, and additives. The main aggregate was coal gangue. Fly ash and cement were binders. Lime, gypsum, and foaming agent were additives [28]. Since it took 40 min for the slurry to reach the far end of the underground filling face from the ground filling and mixing station, the slurry started to set after 60 min. The slurry reaction accelerated after another 50–70 min. After 8 h, the slurry completed its change from liquid to solid. Its compressive strength was then 1.15–2.12 MPa.

3.2. Physical Simulations. To avoid the influence of the F1 fault, the final position of the haulage gate was changed to that shown in Figure 2 when driving the No. 9211 working face. The fault drop was small, and the fault did not conduct water. Meanwhile, the four ash aquifers and five ash aquifers of the roof were drained during excavation. There was no water inrush accident at any time during the excavation process. Therefore, the effect of the fault was not considered in the physical simulation.

This study considered the effect of using PFM to restrain floor water inrush at working face 9211 of the Zhangqiu village coal mine in Shandong Province via physical simulation. The similarity ratio is the critical experimental parameter in simulation experiments that involve similar materials. Choosing a reasonable similarity ratio is an important step in producing valid experimental results. This simulation was based on similarity theory and actual geological conditions and was determined according to the test system. The main similarities were as follows:

(1) *Geometric Similarity*. Suppose that X', Y', and Z' are the three vertical dimensions of the prototype along x, y, z directions, respectively, and suppose X'', Y'', Z'' are the corresponding model sizes along x, y, z directions, respectively,

$$C_l = \frac{X'}{X''} = \frac{Y'}{Y''} = \frac{Z'}{Z''} = 200 \quad (1)$$

(2) *Time Similarity*.

$$C_t = \sqrt{C_l} = 10\sqrt{2} \quad (2)$$

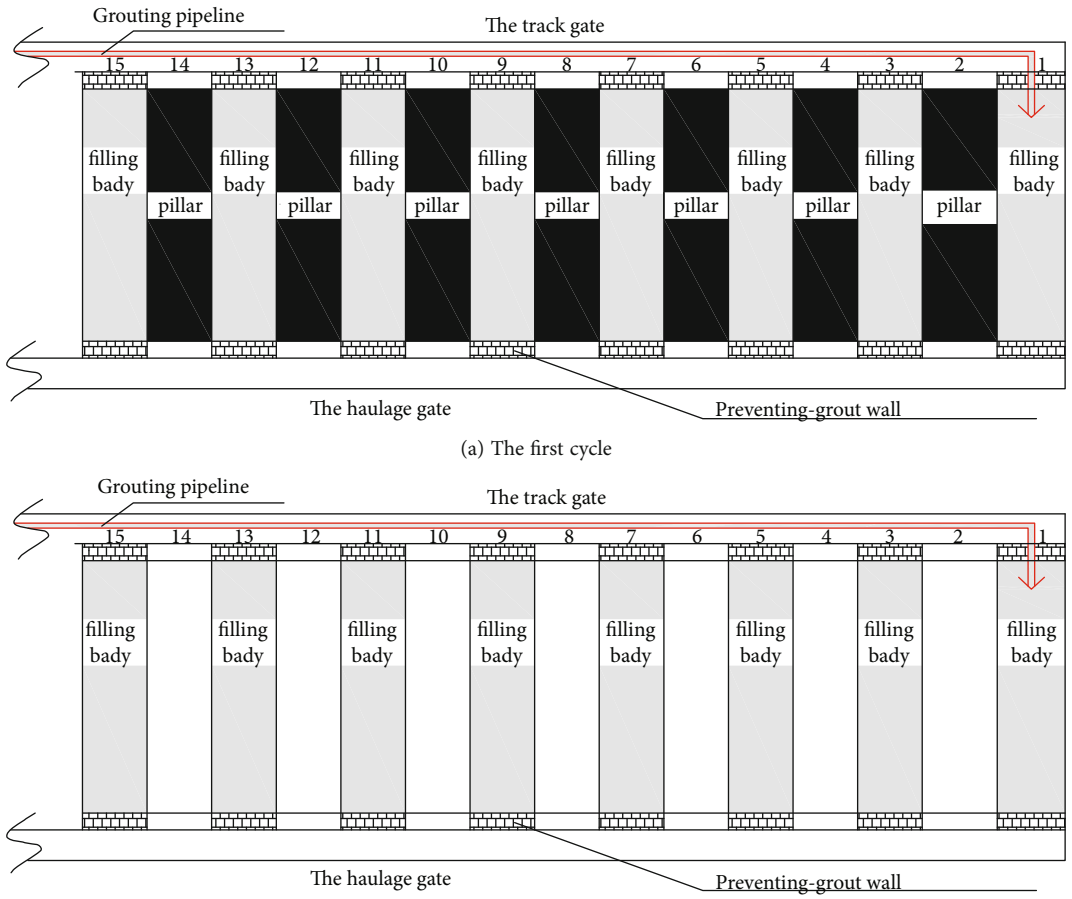

Figure 5: PFM process.

(3) *Bulk Density Similarity*. Let the rock bulk density at the ith layer in the prototype be γ', and the rock bulk density in the corresponding model is γ''. The bulk density similarity coefficient is as follows:

$$C_\gamma = \frac{\gamma'}{\gamma''} = 1.5 \tag{3}$$

(4) *Strength Similarity and Stress Similarity*.

$$C_P = C_l^* C_\gamma = 300 \tag{4}$$

(5) *The Permeability Coefficient Similarity*. Suppose the permeability coefficient is K and the fluid water used in the model is consistent with that in the prototype; therefore, $C_\lambda = 1$, and the permeability coefficient similarity ratio is

$$C_k = \frac{\sqrt{C_1}}{C_\lambda} = 10\sqrt{2} \tag{5}$$

The coal floor water inrush simulation system is composed mainly of a test bench, servo loading system, water pressure control system, and computer acquisition system. The test system is shown in Figure 6. The maximum horizontal load of the servo loading system is 300 kN, the maximum vertical load is 600 kN, the minimum loading rate is 0.01 kN/s, and the maximum loading rate is 100 kN/s. Hydraulic loading is performed mainly by a hydraulic control system. The designed maximum confined water pressure loading value of the system is 1.5 MPa, and the designed maximum flow rate is 0.015 m3/s. The water pressure control system is connected to the test bench water tank via a high-pressure hose. The plunger pump is connected to the water injection head via a high-pressure hose to inject the water from the water tank into the experimental cabin. At the same time, the EDC control system allows the model to achieve multistage, constant water flow control. After the model is prepared, water pressure is applied to it via the water pressure control system until the aquifer is saturated. The water pressure is adjusted automatically via the EDC

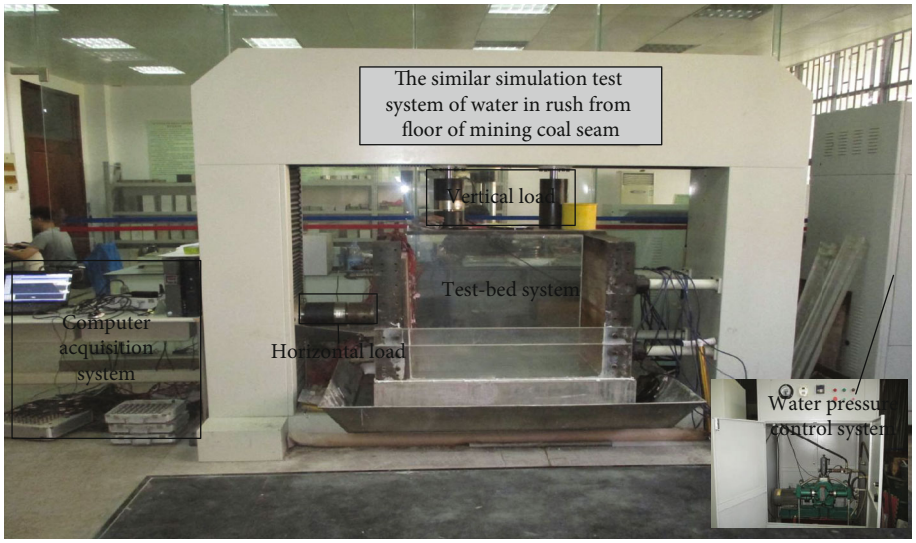

Figure 6: The physical simulation test rig.

Table 1: Physical and mechanical parameters of the strata used in the model.

Rock stratum		Thickness (cm)	Sand (kg)	Calcium carbonate (kg)	Gypsum (kg)	Vaseline (kg)	Paraffin (kg)	Water (kg)	Hydraulic oil (kg)	Actual strength (MPa)	Simulation strength (MPa)
	Limestone	0.45	20.79	2.376	0.594	0	0	2.376	0	62.7	0.209
	Sandy shale	3.5	13.376	1.0032	0.6688	0	0	1.5048	0	42.9	0.143
Main roof	Limestone	0.8	17.325	1.98	1.495	0	0	1.98	0	62.7	0.209
	Fine sandstone	2.5	12.474	0.891	0.891	0	0	1.4256	0	74.9	0.249
	Sandy shale	3.35	8.448	0.6336	0.4224	0	0	0.9504	0	42.9	0.143
Immediate roof	Limestone	0.85	14.08	1.056	0.4224	0	0	1.584	0	62.7	0.209
No. 9 coal seam		0.90	13.86	0.99	0.99	0	0	1.584	0	12.8	0.043
	Fine sandstone	4.3	8.1463	0.8689	0	0.3259	0.1629	0	0.9504	74.9	0.249
	Sandy shale	6.2	12.219	1.3034	0	0.4888	0.2444	0	1.4256	42.9	0.143
	No. 10-1 coal seam	0.6	13.86	0.99	0.99	0	0	1.584	0	12.8	0.043
Water-resisting layer	Clay shale	1.1	13.577	1.4482	0	0.5431	0.2715	0	1.584	32.7	0.109
	Sandy shale	2	10.862	1.1586	0	0.4345	0.2172	0	1.2762	42.9	0.143
	Fine sandstone	2.06	11.541	1.231	0	0.4616	0.2308	0	1.3464	74.9	0.249
	Clay shale	2.5	10.862	1.1586	0	0.4345	0.2172	0	1.6272	32.7	0.109
	Sandy shale	8.55	12.898	1.3758	0	0.5159	0.2580	0	1.5048	42.9	0.143
	Clay shale	3.15	10.183	1.0862	0	0.4073	0.2037	0	1.188	32.7	0.109
Aquifer	Sandstone	3.2	23.936	1.7952	1.0692	0	0	2.5344	0	69.8	0.233
	Limestone	4.1	28.413	1.7758	1.7758	0	0	3.2472	0	62.7	0.209

Figure 7: The construction process of the physical model.

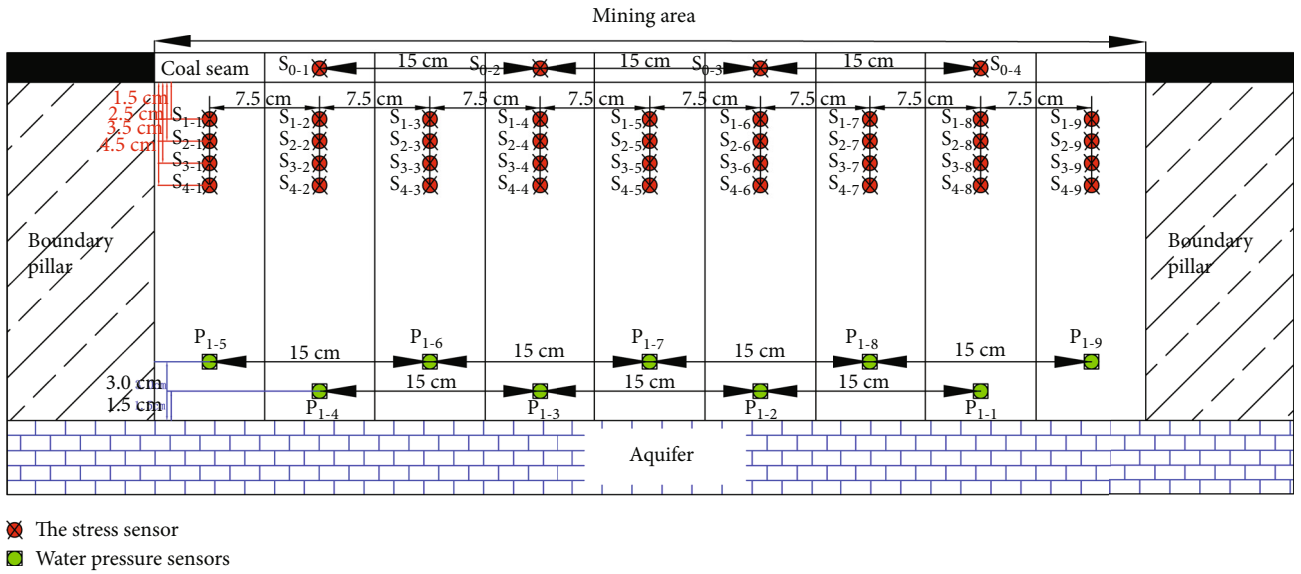

Figure 8: Front view of the monitoring point layout.

control system to ensure that the confined water pressure remains stable during mining.

Based on previous studies, the physical simulation used sand, gypsum, calcium carbonate, and water to simulate the macromotion failures of the overlying strata and the mining floor. The physical and mechanical strata parameters used in the model were determined via similarity theory (Table 1). Figure 7 shows the physical model construction process.

To monitor changes in the stress of the coal seam floor and the water pressure in the aquifer during PFM in real time, stress sensors were placed in the coal seam and in the floor, and water pressure sensors were placed above the aquifer. The arrangement of sensors used in the physical model is shown in Figure 8.

3.3. Test of Specimen Parameters. According to the similarity theory of fluid-solid coupling physical simulation, similar materials in solid-liquid coupling must meet similarity standards for solid deformation and permeability. Four different test schemes were designed in order to verify whether the standard sample of sandy shale prepared from sand, calcium carbonate, paraffin wax, Vaseline, and hydraulic oil could satisfy both the solid deformation and permeability requirements. The material was tested in the dry state and after soaking for 1 d, 2 d, and 3 d. Figure 9 shows the manufacturing processes used with various raw materials and standard samples.

3.3.1. Uniaxial Compressive Strength Test. Figure 10 shows the stress-strain curve of the specimen. The entire stress-

Figure 9: Raw materials and the production process.

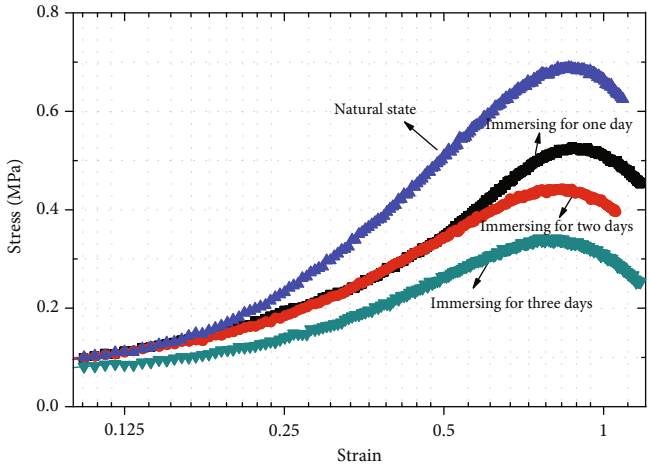

Figure 10: The stress-strain curve.

strain curve is similar to that of rock. However, the strength of the standard specimen decreases with the immersion time. The compressive strength of the hydrophilic specimen can exceed 75% of the specimen strength.

3.3.2. Permeability Coefficient Determination. The permeability coefficient K is one of the indexes that reflects the permeability of the coupling material. In this experiment, the permeability coefficient K of the coupling material is measured via the variable-head method. Diagrams of the test principle and test device are shown in Figure 11 [31]. The test instructions are as follows: first, put the saturated sample into a closed steel container for compaction; second, record the water head difference in the U-shaped pipe at the beginning of the test as Δh_1; third, record the water head difference in the U-shaped pipe after time t as Δh_2; fourth, calculate the permeability coefficient of the test piece according to Darcy's law. The formula for the permeability coefficient is

$$K = \frac{aL}{At} \ln \frac{\Delta h_1}{\Delta h_2}, \tag{6}$$

where K is the permeability coefficient, a is the cross-sectional area of the glass pipe, A is the cross-sectional area of the sample, L is the length of the sample, Δh_1 is the water head difference of the U-shaped pipe at time t_1, and Δh_2 is the water head difference of the U-shaped pipe at time t_2.

Coupling material permeability measurements performed using various proportions indicate that the permeability coefficient range is 4.55×10^{-4} to 1.48×10^{-7}. The permeability coefficient values of some materials are shown in Table 2.

3.4. Field Measurements. Field monitoring is an important way to verify the results of physical simulations and analyses. To verify the preventive effect of PFM with respect to floor water inrush accidents, stress and roof subsidence gauges were arranged in the filling area, transportation chute, and track chute of a narrow-strip working face. There were three pairs of measuring points in the filling area of the narrow-strip face. Roof subsidence gauges were placed along the transport and track chutes. The stress and roof subsidence gauges in the filling area of the narrow-strip working face were 25 m, 50 m, and 75 m from the No. 9211 haulage gate. The roof subsidence gauges in the transport and track grooves were 105 m away from the cutting hole of the working face. The sensor layout is shown in Figure 12.

The failure depth of the floor after coal seam mining was verified via the observation method using a double-end water shutoff device. The system has two pathways in the structure: the gas filling pathway and the water injection pathway. The inflatable pathway is composed of a high-pressure gas cylinder inflatable console and an in-hole blocking capsule; the water injection pathway is composed of high-pressure water, a water injection console, a water inlet push rod, and an in-hole water injection probe tube. First, gas is applied to the capsule at a certain pressure through the inflatable path so that the capsule expands and seals the two ends of the section where the hole is located. Then, constant-pressure water is injected into the blocked section of the capsule via the water injection path. The water

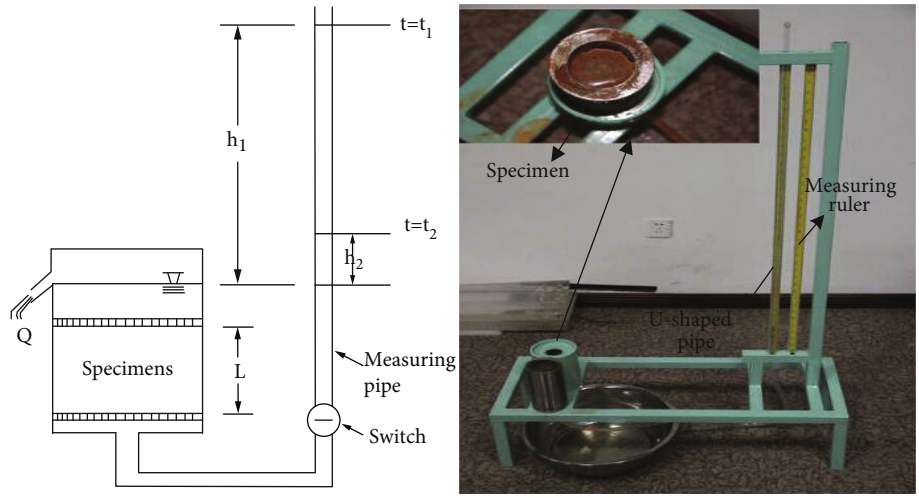

Figure 11: The permeability coefficients of some specimens.

Table 2: The permeability coefficients of some specimens.

Specimen number	K (cm/s)	Specimen number	K (cm/s)
1-3	5.86×10^{-5}	5-3	7.31×10^{-6}
2-3	4.75×10^{-4}	6-3	5.07×10^{-5}
3-3	6.02×10^{-5}	7-3	4.55×10^{-4}
4-3	4.56×10^{-6}	8-3	1.48×10^{-7}

pressure is controlled by the water injection console, and the water injection flow rate is monitored. The capsule of the blocker is depressurized after each hole section measurement. After contraction and depressurization, the procedure moves to the next measurement section and water injection observation continues until the leakage from each section of the entire borehole is measured, and the bottom plate fracture damage range is determined based on the change in leakage amount. A schematic diagram of water injection in the damaged floor area is shown in Figure 13 [32].

The water injection holes constructed before and after mining in the No. 9211 working face include one premining hole (hole No. 3) and two postmining holes (holes No. 1 and No. 2). Construction of and observations via the premining hole were performed without affecting mining. The drilling holes were protected when drilling the two postmining holes. Finally, the water lost into the pre- and postmining holes was measured using a double-end water shutoff device to determine the floor failure depth. Figure 14 shows the drilling elevation plan.

4. Results and Discussion

4.1. Physical Simulations. After the model was built, the vertical stress, horizontal stress, and confined water pressure were considered based on similarity theory. The model is maintained at room temperature for 4–5 days before excavation. To reduce the boundary effect, coal pillars 5 cm wide are retained on both sides of the model. The coal seam in the model is mined using PFM. The mining face and the pillar widths are both 7.5 cm. The working face is mined from the left end to the right end of the model. There are six periods of mining, each lasting 40 min. The goaf is filled 10 min after completion of each excavation. The pillars between fillings are extracted in turn from the left end of the model after mining of the working face is completed. In the physical simulation, mining of the coal seam uses manual drilling and the backfill body is foam. Figure 15(a) shows the initial physical model. Figures 15(b) and 15(c) show the first and second cycles of PFM, respectively.

In order to analyze the stress and water pressure variation laws relevant to simulated mining, data from stress monitoring points S1-3, S2-5, S3-5, and S4-5 and the data from pore water pressure monitoring points P1-4 and P1-8 are selected for analysis.

4.1.1. Evolution of the Stress Field during Mining. Data from stress sensor S1-3 are shown in Figure 16(a) for the first cycle of mining. The stress changes three times. The first change occurs during continuous excavation of the working face. The stress measured by the sensor at the lower 1.5 cm of the working face changes abruptly, increasing from 0 MPa to 0.031 MPa. This occurs mainly because the floor rock stratum in this area begins to move towards the goaf due to vertical stress and mine pressure after excavation of the working face. The rock stratum is in tension.

The second step change occurs during the filling step, after excavation of the working face has been completed. The stress in the rock floor gradually decreases to that of the rock floor mass without excavation. This change indicates that the weight of the roof rock stratum of the coal seam is beginning to transfer to the floor rock stratum through the filling body. This restrains the upward movement of the rock stratum.

The third step change occurs during compaction of the filler. The stress changes from 0 MPa to -0.01 MPa, indicating that the filling body in the goaf is in contact with the roof

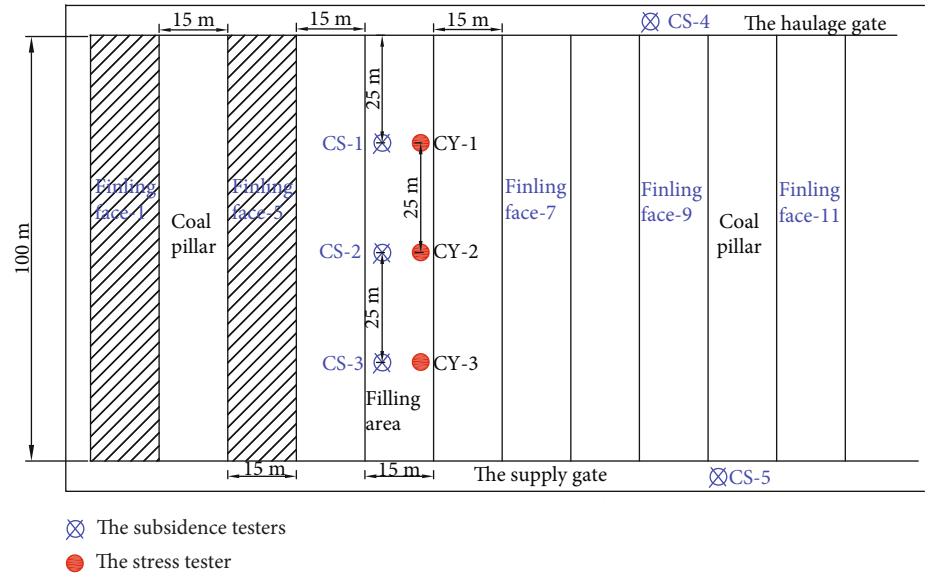

Figure 12: Layout of stress and subsidence gauges.

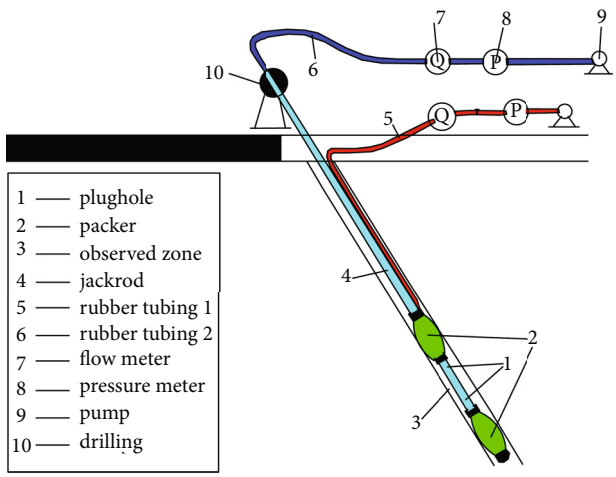

Figure 13: Schematic diagram of water injection in the damaged area of the mining floor.

and that the floor rock stratum is in compression again. This reduces the floor rock stratum failure depth.

In Figure 16(b), during the second mining cycle, the stress measured by the floor sensor 1.5 cm away from the coal seam indicates compression. The stress is higher than that at the end of the first excavation. This indicates that the floor rock layer is affected by excavation again.

The stress measured by sensor S2-5, which is 2.5 cm away from the coal seam, is always compressive during the first excavation period (Figure 17). The stress decreases during the second excavation. This occurs primarily because unloading occurs in the floor strata when the coal pillars are extracted. However, stress sensors S3-5 and S4-5 are always under pressure during the two rounds of excavation. Based on a similar material ratio of the laying model of 1 : 200, the floor failure depth would be less than 5 m during mining.

4.2. Evolution of the Pore Water Pressure during Mining. Data from water pressure sensor P1-4 (Figure 18) show that the initial water pressure increases from 0 MPa to -0.04 MPa during the two excavations. It then fluctuates between -0.03 and -0.04 MPa. This occurs mainly because the primary fissures in the rock strata open to form a water conduction channel under a sustained high confined water pressure. This produces a water flow that is measured by the water pressure sensor. Therefore, a water-conducting channel forms 1.5 cm above the aquifer due to the action of the confined water pressure.

Data from water pressure sensor P1-8 are shown in Figure 19. The sensor, which is 3.0 cm from the aquifer, is affected by the water pressure throughout PFM. The data from P1-8 show that under the action of high confined water and mine pressures, rock fractures develop to a height of 3.0 cm above the aquifer. This occurs mainly because the water pressure, as measured by the sensor, fluctuates continuously upwards and then falls to 0 MPa. This shows that the rock stratum is not completely broken.

The variation in the stress measured by water pressure sensors P1-4 and P1-8 shows that throughout mining of the No. 9211 working face, the height of the hydraulic conductivity lifting zone under long-term confined water pressure and mine pressure loads is less than 3.0 cm.

Layered demolition was used to measure the development and expansion of cracks in the upper aquifer of the floor during excavation. When the first, second, and third layers above the aquifer were dismantled, the fractures shown in Figures 20(a) and 20(b) appeared. This indicates that floor rock fractures expand during coal seam mining due to pressure from the mine and the confined water. The similarity ratio indicates that the height of the confined water conduction lifting zone would increase by less than 6 m.

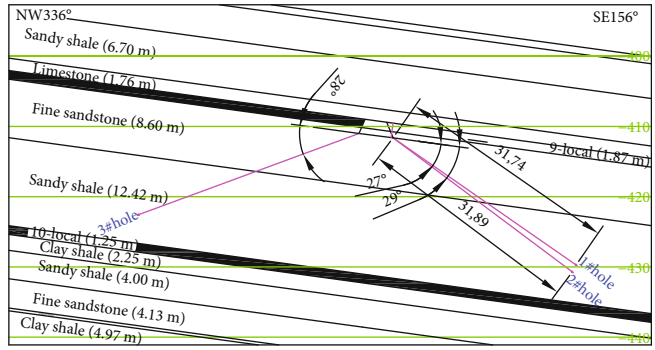

Figure 14: Drilling elevation plan.

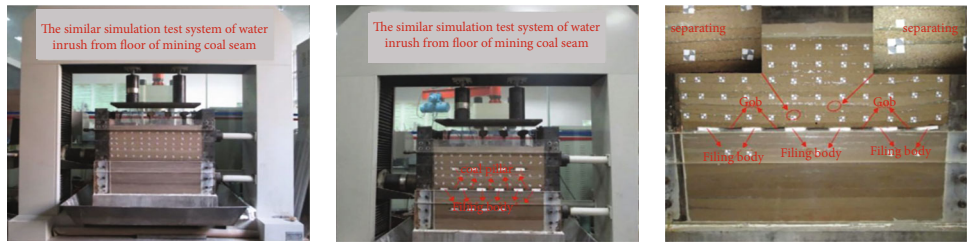

(a) (b) (c)

Figure 15: Excavation in the physical model.

4.3. Field Application

4.3.1. Compression Deformation of Filling Body in Mining. According to data from subsidence gauges CS-1, CS-2, and CS-3, compression of the filling body in the No. 9211 working face can be divided into two stages. The first stage is compressive deformation of the filling body (Figure 21). Compression of the high-water backfill in the No. 9211 working face is linear with time. The compressive deformation measured by CS-2, in the middle of the goaf, is the largest at 89.1 mm for the filling body. This occurs mainly because the early strength of the high-water backfill is relatively low and the support for the overlying strata is weak. This leads to subsidence of the rock strata and backfill compression. Therefore, the backfill compression is linear with time. The filling body is stable during the second stage. This is mainly because the strength of the filling body, which has high water content, increases. This increases support of the overlying strata and decreases the extent of strata settlement. Thus, compression of the filling body becomes stable.

The CS-5 and CS-4 subsidence gauges are in the track and transport chutes, respectively. Data from these sensors indicates that variation in compression can be divided into two stages (Figure 21). In the first stage, the compression increases, mainly because the roof stratum along the trough sinks is under mine pressure after the excavation of the coal body at the working face. The second stage is stable. The compression measured by CS-5 is larger than that measured by CS-4. This is mostly because CS-5 is on one side of a coal pillar.

4.3.2. Stress Evolution within the Filling Body during Mining. As shown in Figure 22, data from the CY-1, CY-2, and CY-3 pressure sensors in the goaf show that the pattern of stress in the filling body can be divided into two stages. Loading of the filling body increases during stage 1 but is stable during stage 2. The stress measured by sensor CY-2 is larger than that measured by the CY-1 and CY-2 sensors. This indicates that the filling body experiences a larger force in the middle of the goaf.

The depth of the No. 9211 working face is 430.26 m–484.96 m. Without considering the tectonic stress, the original rock stress is 4.61 MPa–5.20 MPa. The pressure on the filling body is 0.51 MPa in the middle of the working face and 0.32 MPa in the upper face. Therefore, the stress in a high-water filling body is less than the original rock stress of the working face. This indicates that movement of the rock strata above the working face is limited at this time. Therefore, PFM can inhibit the occurrence of strata breakage, thereby reducing the effect of the overlying strata pressure on the floor.

4.3.3. Floor Failure Depth during Mining. Using the drilling construction layout shown in Figure 14, floor damage depth observation was performed at the No. 9211 working face. The observation period was from July 15, 2013, to July 22, 2013. Water injection leakage results measured at various drilling depths during drilling are shown in Figure 23.

In Figure 14, the strata that the premining hole (S-3) passes through are mainly sandy shale and fine sandstone from the floor rock of the 9-1 coal seam. According to the water injection leakage diagram, the extent of leakage from the premining hole (S-3) decreases gradually from 11 m to 18 m. Leakage is maximized at a depth of 11 m, where the maximum leakage is 2.6 L/min and the corresponding rock

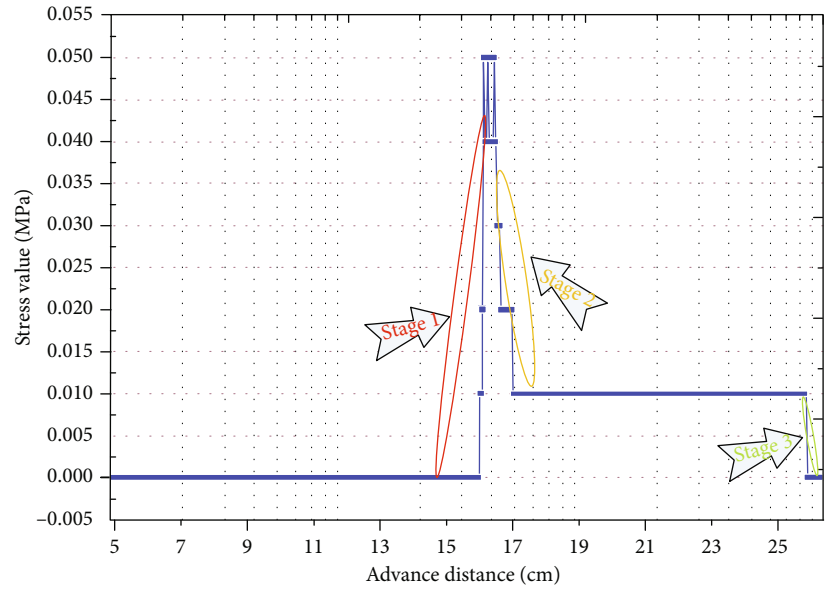

(a) The first cycle

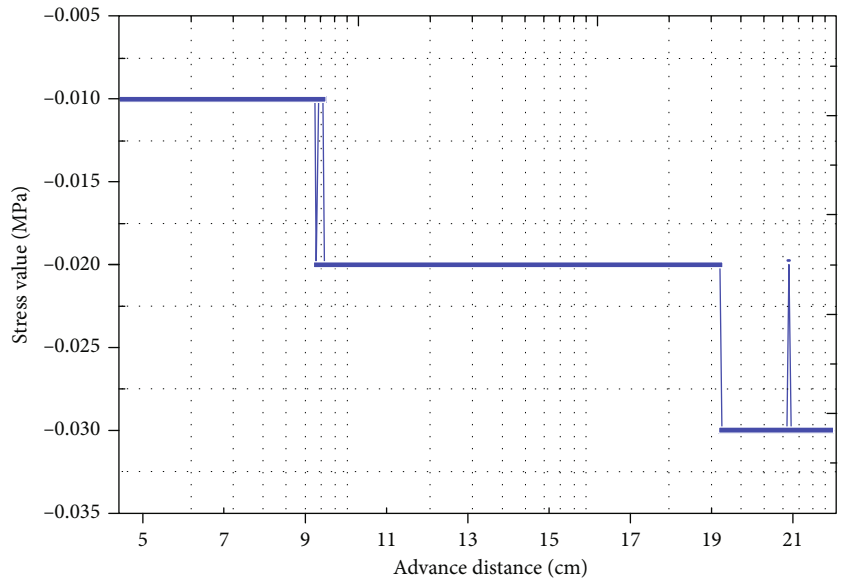

(b) The second cycle

Figure 16: Stress at monitoring point S1-3 vs. the distance advanced.

layer position of the fine floor sandstone is 5.16 m. The drilling depth ranges from 19 m to 31 m, and the corresponding rock layer is sandy shale. Due to the relatively complete rock stratum, the extent of leakage from the drilling section is stable within a relatively small range. The maximum leakage is 1.3 L/min. Across the borehole, the average leakage from the premining hole (S-3) is 1.39 L/min.

It can be seen from Figure 23 that drilling leakage from the postmining hole (S-1) between 8 m and 13 m is relatively stable at about 17.3 L/min. The maximum leakage of 18.0 L/min occurs at 13 m. The corresponding rock stratum at the maximum leakage location is 5.90 m of fine floor sandstone. From 14 m to 17 m, the corresponding strata are fine sandstone and sandy shale. The drilling leakage decreases from 18 L/min to 6.2 L/min, and the floor failure depth is 7.72 m. From 18 m to 30 m, the corresponding stratum is sandy shale, and the leakage is always less than 2 L/min. The average leakage across the entire borehole is 6.82 L/min.

The maximum leakage at S-2 between 8 m and 11 m is 18.3 L/min and occurs at 11 m. The corresponding rock stratum of the maximum leakage location is 5.33 m of fine floor sandstone. Between depths of 11 m and 17 m, leakage decreases from 18.3 L/min to 6.1 L/min. At depths of 17 m to 30 m, leakage is stable below 2 L/min. The average leakage across the entire borehole is 5.82 L/min.

According to the statistical analysis of water leakage at the three boreholes, the maximum and average leakage at the premining hole (S-3) are smaller than those at the

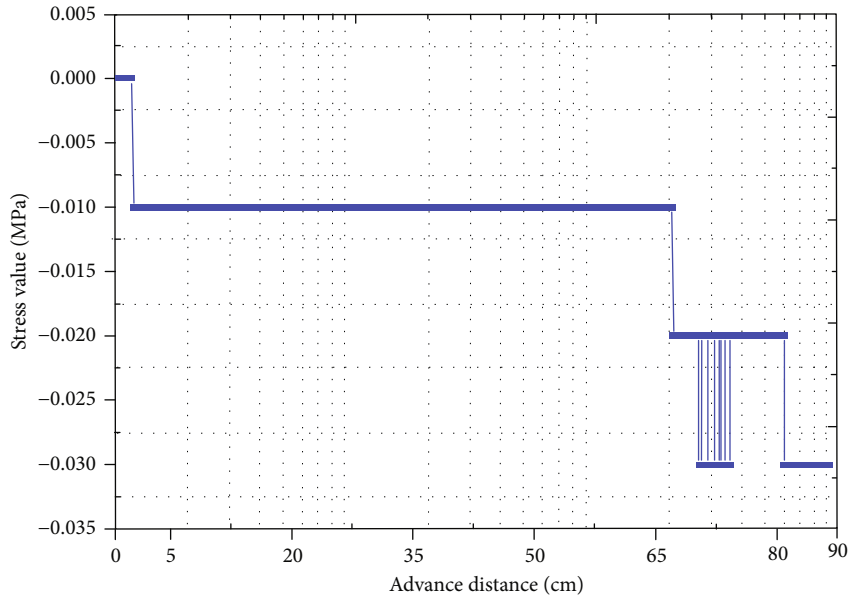

(a) The first cycle

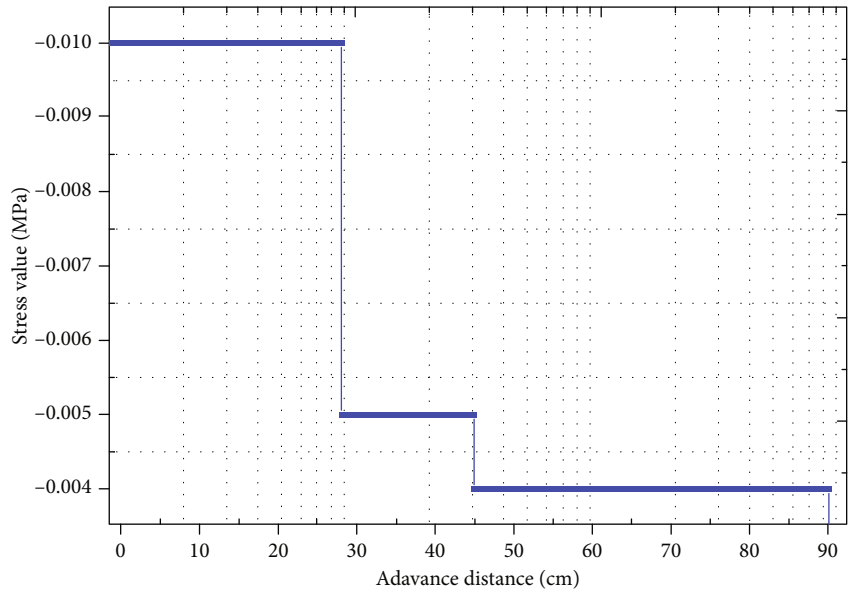

(b) The second cycle

Figure 17: Stress at monitoring point S2-5 vs. the distance advanced.

postmining holes (S-1 and S-2). In addition, analysis of the location of maximum leakage at the postmining holes (S-1 and S-2) and the drilling leakage attenuation process indicates that the fine floor sandstone is damaged and the sandy shale is nearly complete in the process of using PFM in 9211 working face.

4.4. Comparative Analyses. Analysis of the PFM mining process via the similar material simulation experimental method indicates that the overlying rock does not exhibit bubbling down during mining. The overlying rock layer develops microfractures and delamination from the top plate upward, and the fracture stops developing when it reaches approximately 6 times the mining height above the top plate. The overlying rock layer shows the overall bending and sinking phenomenon, and the open fissures formed by mining gradually close with bending and sinking of the rock layer. Therefore, the PFM process avoids formation of a large fissure channel in the roof plate that can cause roof aquifer water to gush into the mining area. At the same time, the laminar demolding method adopted at the end of the simulated excavation reveals that the coupled support system comprised of a top plate, filling body, and bottom plate formed by the PFM mining system transfers the pressure

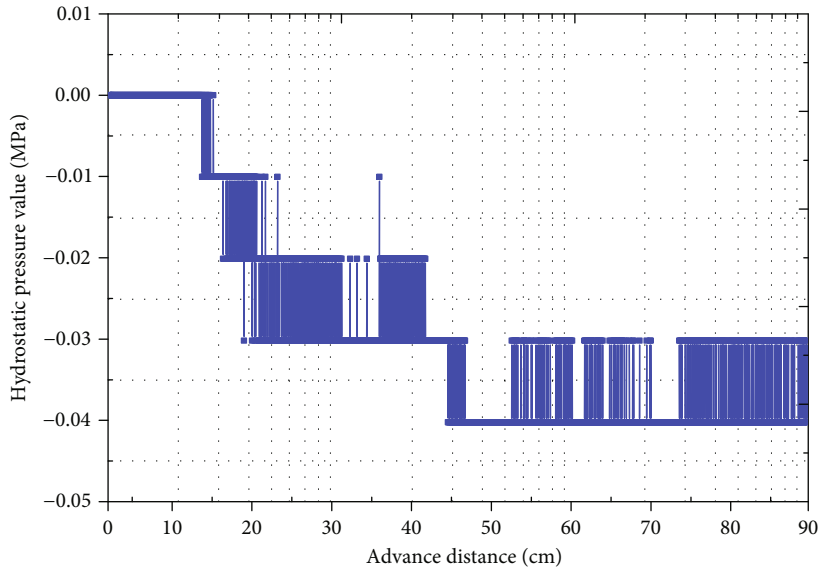

Figure 18: Pore water pressure at monitoring point P1-4 vs. the distance advanced.

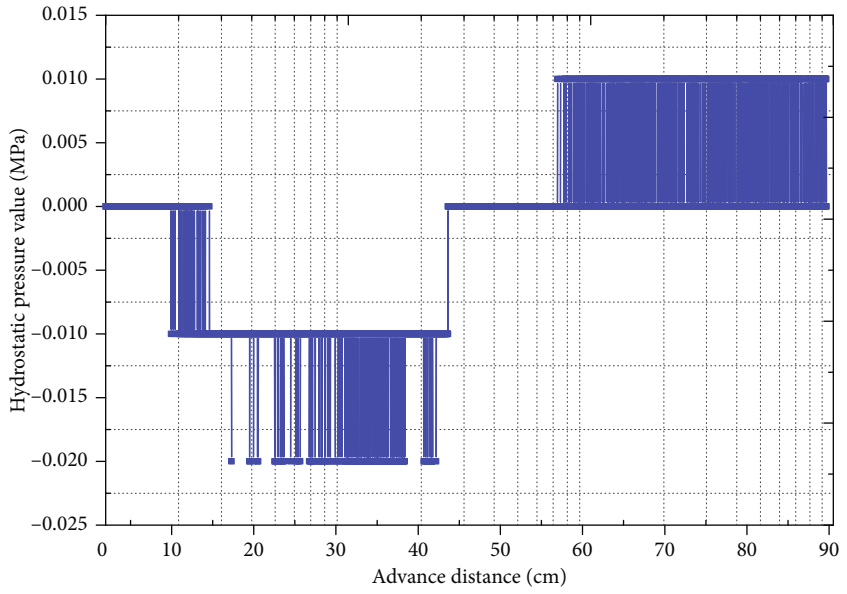

Figure 19: Pore water pressure at monitoring point P1-8 vs. the distance advanced.

of the overlying rock layer to the bottom plate via the filling body. This prevents the bottom plate rock layer from moving to the mining void area. The damage depth of the bottom plate is less than 5 m. Thus, the damage depth of the bottom plate rock layer is reduced, and the effective water barrier thickness of the bottom plate is increased.

In order to provide more accurate feedback on the effectiveness of the PFM method in preventing and controlling sudden bottom slab water, stress and top slab sinkage monitors were arranged in the filling area, transport chute, and track chute of the working face when the method was applied to working face 9211. The actual deformation of the top and bottom plates in the middle and end of the working face is approximately 80.8 mm and 57.4 mm, respectively. Based on the attenuation coefficient of the overlying rock layer, the actual surface deformation is expected to be approximately 56.6 mm and the surface building may be controlled within the Class I damage deformation. At the same time, it is known from the double-end plugger field measurement that the bottom slab damage depth range occurs within the siltstone. The lowest point of the bottom slab fracture development starts 8.95 m from the coal seam

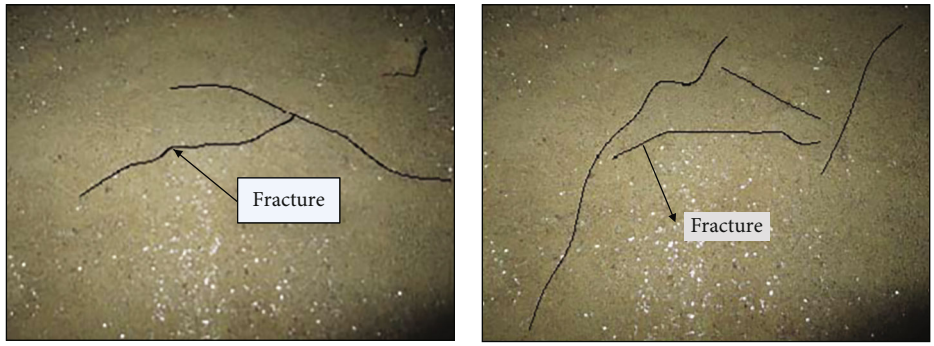

(a) The third layer (b) The second layer

Figure 20: Crack growth and expansion.

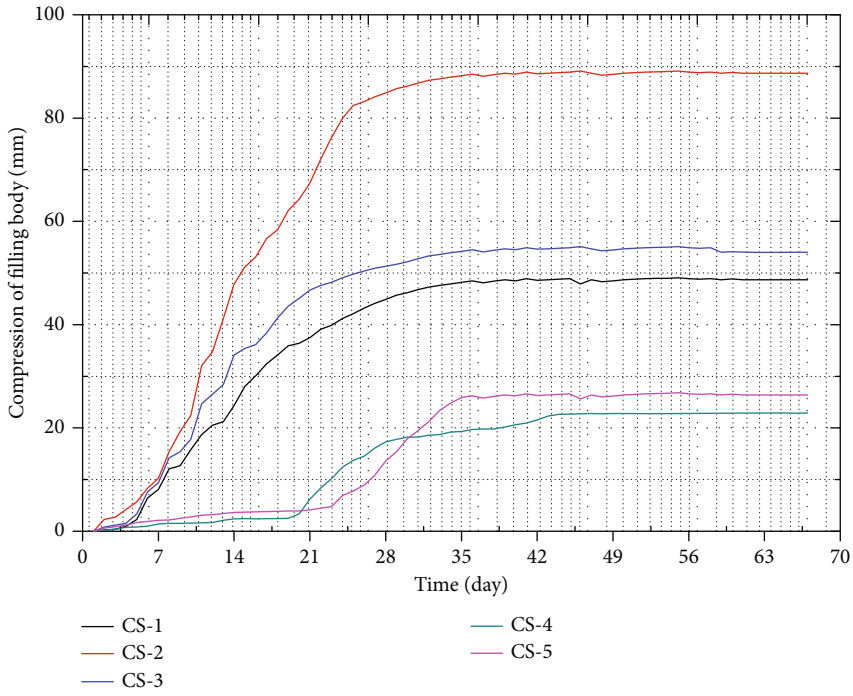

Figure 21: Compressive deformation of the paste backfill body vs. the curing age.

floor. However, according to the empirical formula (7) for the bottom slab damage zone used by the researchers, the bottom slab damage depth is 20.30 m when working face 9211 is mined via the conventional collapse method. Therefore, using this PFM method reduces the bottom slab damage depth by 11.35 m compared to the traditional collapse method. The hydrogeological conditions suggest that the effective water barrier thickness of the bottom slab of working face 9211 after completion of PFM mining is 50.85. According to formula (8), which uses the sudden water coefficient method, the sudden water coefficient is 0.08 MPa/m, which is less than 0.1 MPa/m and therefore safe. The effective water barrier thickness is 50.85:

$$h = 0.0085H + 0.1664\alpha + 0.1079L + 4.3597, \quad (7)$$

where H is the coal seam burial depth, which is taken to be 420 m in this paper; α is the coal seam dip angle, which is taken to be 9.5°; and L is the working face slope length, which is taken to be 100 m:

$$T = \frac{P}{M}, \quad (8)$$

where P is the bottom plate water barrier water pressure limit, which is taken to be 4.11 MPa, and M is the bottom plate water barrier effective thickness, which is taken to be 50.85 m.

In summary, the PFM method can not only effectively control the depth of bottom damage but also consume coal gangue to protect the mine environment and can be promoted and applied under similar conditions.

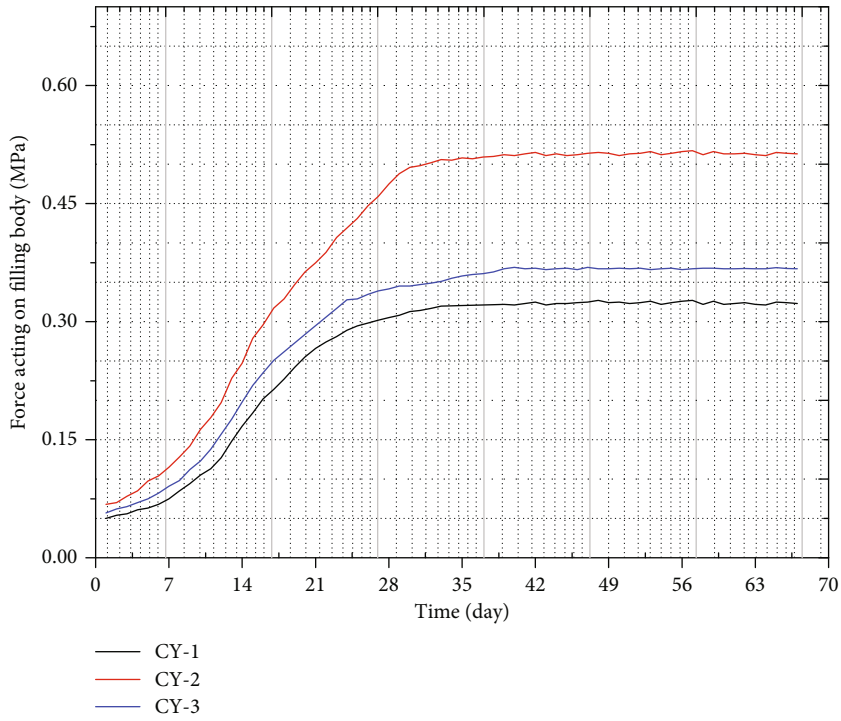

Figure 22: Force acting on the paste backfill body vs. the curing age.

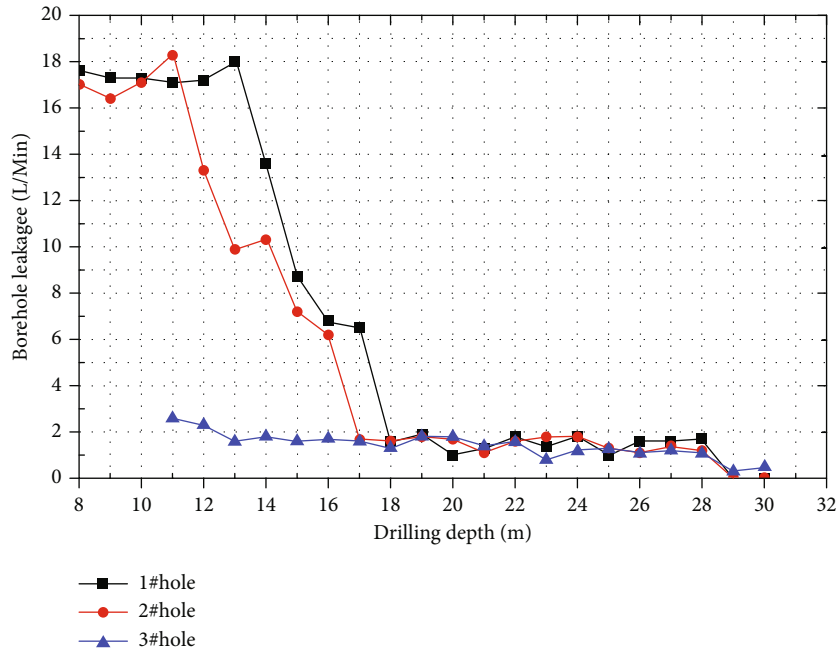

Figure 23: Amount of borehole water leakage.

5. Conclusions

Using the hydrogeological conditions of the No. 9211 working face of the Bucun Coal Mine, this paper presented PFM as a method of preventing water from inrushing from the floor. The feasibility of PFM was verified via indoor physical simulation tests and field application. Unlike the traditional water control method, this PFM method considers the relationship between the ground pressure and floor rock mass failure. In addition, coal gangue serves as the main aggregate and fly ash as the main cementing agent; they not only play the role of filling materials but also eliminate the negative impacts of fly ash and coal gangue on the environment. Therefore, this method can be used to prevent and control mine water disasters.

Data Availability

All data, models, and code generated or used during the study appear in the submitted article. For any questions or need for more detailed data, please contact the corresponding author of this article.

Conflicts of Interest

The authors declare that they have no conflicts of interest.

Acknowledgments

This study was supported by the National Natural Science Foundation of China (grants 51574159, 51428401, and 41702270), the Science and Technology Innovation and Entrepreneurship Fund Special Project of Tiandi Science and Technology Co., Ltd. (2019-td-ms004), the Youth Science Fund Project of National Natural Science Fund (51704161), the Shandong Province Natural Science Foundation (grant ZR2014EEM001), and a postdoctoral fund (grants 2015M572068 and 2016T90662).

References

[1] M. Christopher and G. Michael, "Evaluating the risk of coal bursts in underground coal mines," *International Journal of Mining Science and Technology*, vol. 26, no. 1, pp. 47–52, 2016.

[2] W. Y. Guo, T. B. Zhao, Y. L. Tan, F. H. Yu, S. C. Hu, and F. Q. Yang, "Progressive mitigation method of rock bursts under complicated geological conditions," *International Journal of Rock Mechanics and Mining Sciences*, vol. 96, pp. 11–22, 2017.

[3] G. N. Muriithi, L. F. Petrik, W. M. Gitari, and F. J. Doucet, "Synthesis and characterization of hydrotalcite from South African coal fly ash," *Powder Technology*, vol. 312, pp. 299–309, 2017.

[4] S. Vahab and T. Abdollah, "Numerical simulation of the influence of interaction between qanat and tunnel on the ground settlement," *Geomechanics and Engineering*, vol. 23, no. 5, pp. 455–466, 2020.

[5] S. N. Dong, H. Wang, and W. Z. Zhang, "Judgement criteria with utilization and grouting reconstruction of top Ordovician limestone and floor damage depth in North China coal field," *Journal of China Coal Society*, vol. 44, no. 7, pp. 2216–2226, 2021.

[6] S. C. Li, J. Wu, Z. H. Hu, and W. M. Yang, "Mechanics criterion of water inrush from the coal floor under influence of fault and its engineering application," *International Journal of Geomechanics*, vol. 19, no. 5, 2019.

[7] B. Fang, "Method for quickly identifying mine water inrush using convolutional neural network in coal mine safety mining," *Wireless Personal Communications*, 2021.

[8] S. L. Liu, W. T. Liu, and J. J. Shen, "Stress evolution law and failure characteristics of mining floor rock mass above confined water," *KSCE Journal of Civil Engineering*, vol. 21, no. 7, pp. 2665–2672, 2017.

[9] Z. P. Meng, G. Q. Li, and X. T. Xie, "A geological assessment method of floor water inrush risk and its application," *Engineering Geology*, vol. 143-144, pp. 51–60, 2012.

[10] W. C. Song and Z. G. Lian, "Theoretical and numerical investigations on mining-induced fault activation and groundwater outburst of coal seam floor," *Bulletin of Engineering Geology and the Environment*, vol. 76, no. 23, pp. 1–15, 2021.

[11] L. L. Xiao, Q. Wu, C. Niu et al., "Application of a new evaluation method for floor water inrush risk from the Ordovician fissure confined aquifer in Xiayukou coal mine, Shanxi, China," *Carbonates and Evaporites*, vol. 35, no. 3, 2020.

[12] J. W. Cheng, G. Zhao, G. R. Feng, and S. Y. Li, "Characterizing strata deformation over coal pillar system in longwall panels by using subsurface subsidence prediction model," *European Journal of Environmental and Civil Engineering*, vol. 24, no. 5, pp. 650–669, 2020.

[13] H. Karimi, E. Raeisi, and M. Bakalowicz, "Characterising the main karst aquifers of the Alvand basin, northwest of Zagros, Iran, by a hydrogeochemical approach," *Hydrogeology Journal*, vol. 13, no. 5-6, pp. 787–799, 2005.

[14] G. Panagopoulos, N. Lambrakis, C. Katagas, D. Papoulis, and P. Tsolis-Katagas, "Water–rock interaction induced by contaminated groundwater in a karst aquifer, Greece," *Environmental Geology*, vol. 49, no. 2, pp. 300–313, 2005.

[15] C. S. Wang, Y. J. Jiang, R. C. Liu, C. Wang, Z. Y. Zhang, and S. Satoshi, "Experimental study of the nonlinear flow characteristics of fluid in 3D rough-walled fractures during shear process," *Rock Mechanics and Rock Engineering*, vol. 5, no. 6, pp. 2581–2604, 2020.

[16] Z. Z. Cao, Y. L. Ren, Q. T. Wang, B. H. Yao, and X. C. Zhang, "Evolution mechanism of water-conducting channel of collapse column in karst mining area of southwest China," *Geofluids*, vol. 2021, 8 pages, 2021.

[17] Y. L. Lu and L. G. Wang, "Numerical simulation of mining-induced fracture evolution and water flow in coal seam floor above a confined aquifer," *Computers and Geotechnics*, vol. 67, pp. 157–171, 2015.

[18] S. L. Liu, S. Dai, W. P. Li, B. Han, B. He, and J. P. Luo, "A new monitoring method for overlying strata failure height in Neogene laterite caused by underground coal mining," *Engineering Failure Analysis*, vol. 117, article 104796, 2020.

[19] B. L. Zhang and Z. B. Meng, "Experimental study on floor failure of coal mining above confined water," *Arabian Journal of Geosciences*, vol. 12, no. 4, 2019.

[20] L. W. Chen, X. Q. Feng, D. Q. Xu, W. Zeng, and Z. Y. Zheng, "Prediction of water inrush areas under an unconsolidated, confined aquifer: the application of multi-information superposition based on GIS and AHP in the Qidong Coal Mine, China," *Mine Water and the Environment*, vol. 37, no. 4, pp. 786–795, 2018.

[21] Q. X. Gu, Z. Huang, S. J. Li, W. Zeng, Y. Wu, and K. Zhao, "An approach for water-inrush risk assessment of deep coal seam mining: a case study in Xinlongzhuang coal mine," *Environmental Science and Pollution Research*, vol. 27, no. 34, pp. 43163–43176, 2020.

[22] W. B. Sun, R. Malekian, J. C. Yu, X. H. Feng, and Z. X. Liu, "Electrical anisotropic response of water conducted fractured zone in the mining goaf," *IEEE Access*, vol. 4, pp. 6216–6224, 2016.

[23] M. Z. Naghadehi, R. Mikaeil, and M. Ataei, "The application of fuzzy analytic hierarchy process (FAHP) approach to selection of optimum underground mining method for Jajarm Bauxite Mine, Iran," *Expert Systems With Applacations*, vol. 36, no. 4, pp. 8218–8226, 2009.

[24] X. Guo, J. R. Chai, Y. Qin, Z. G. Xu, Y. N. Fan, and X. W. Zhang, "Mechanism and treatment technology of three water

inrush events in the Jiaoxi River Tunnel in Shaanxi, China," *Journal of Performance of Constructed Facilities*, vol. 33, no. 1, 2019.

[25] A. Li, Y. Liu, L. Mou, and K. Li, "Numerical analysis and case study on the mitigation of mining damage to the floor of no. 5 coal seam of Taiyuan Group by grouting," *Journal of the Southern African Institute of Mining and Metallurgy*, vol. 118, no. 5, pp. 461–470, 2018.

[26] E. Jaouhar, L. Li, and M. Aubertin, "An analytical solution for estimating the stresses in vertical backfilled stopes based on a circular arc distribution," *Geomechanics and Engineering*, vol. 15, no. 3, pp. 889–898, 2018.

[27] N. Jiang, C. X. Wang, H. Y. Pan, D. W. Yin, and J. B. Ma, "Modeling study on the influence of the strip filling mining sequence on mining-induced failure," *Energy Science and Engineering*, vol. 8, no. 6, pp. 2239–2255, 2020.

[28] M. G. Karfakis, C. H. Bowman, and E. Topuz, "Characterization of coal-mine refuse as backfilling material," *Geotechnical and Geological Engineering*, vol. 14, no. 2, pp. 129–150, 1996.

[29] Y. M. Qi, J. Y. Tian-Chyi, Y. C. Wu, M. Li, and Y. H. Hao, "Comparing control methods of water inrush disaster using mathematical programming: modelling, analysis and a case study," *Geomatics Natural Hazards and Risk*, vol. 8, no. 2, pp. 1869–1885, 2017.

[30] W. H. Sui, J. Y. Liu, S. G. Yang, Z. S. Chen, and Y. S. Hu, "Hydrogeological analysis and salvage of a deep coalmine after a groundwater inrush," *Environmental Earth Sciences*, vol. 62, no. 4, pp. 735–749, 2011.

[31] J. T. Chen, L. M. Yin, W. B. Sun, C. Lu, S. C. Zhang, and X. Z. Sun, "Development and application of new deep solid fluid coupling similar materials," *Chinese Journal of Rock Mechanics and Engineering*, vol. 34, no. 2, pp. 3956–3964, 2015.

[32] J. H. Zhao, J. T. Chen, X. G. Zhang, N. Jiang, and Y. Z. Zhang, "Distribution characteristics of floor pore water pressure based on similarity simulation experiments," *Bulletin of Engineering Geology and the Environment*, vol. 79, no. 9, pp. 4805–4816, 2020.